



**A Search for  $ZH(\rightarrow e^+e^-b\bar{b})$  and  $ZH(\rightarrow \mu^+\mu^-b\bar{b})$  Production  
with the DØ Detector in  $p\bar{p}$  Collisions at  $\sqrt{s} = 1.96$  TeV**

The DØ Collaboration  
URL <http://www-d0.fnal.gov>  
(Dated: July 31, 2008)

We report on a search for a Higgs boson produced in association with a  $Z$  boson in  $2.3 \text{ fb}^{-1}$  of  $p\bar{p}$  collisions at  $\sqrt{s} = 1.96$  TeV at the Fermilab Tevatron collider. Events containing a  $Z \rightarrow e^+e^-$  or  $\rightarrow \mu^+\mu^-$  and two jets where at least one jet is  $b$ -tagged are considered. The observed data are consistent with the expected background. Upper limits on the  $ZH$  production cross section are set for Higgs masses between 100 and 140 GeV. The limit for the full Run II dataset is about 11 times the standard model prediction for a  $m_H = 115$  GeV.

*Preliminary Results for Summer 2008 Conferences*

## I. INTRODUCTION

One of the most sensitive search channels at the Tevatron for a standard model Higgs boson with a mass below approximately 140 GeV is the associated production of a Higgs boson with a  $Z$  boson with the Higgs decaying to  $b\bar{b}$ . In this note we present a search for  $ZH$  production in  $\ell^+\ell^-b\bar{b}$  final states where  $\ell = e, \mu$ . The product of cross section and branching fraction ( $\sigma(p\bar{p} \rightarrow ZH) \times B(H \rightarrow b\bar{b})$ ) is predicted to be  $14 - 0.75 \text{ fb}$  [1] for a standard model Higgs boson with a mass between 100 and 140 GeV.

The  $Z$  boson is reconstructed and identified from a pair of high  $p_T$  electrons or muons with an invariant mass requirement. Events are required to have at least two jets and at least one of the jets identified as a  $b$  jet (we refer to such jets as  $b$ -tagged). We then search for a  $H \rightarrow b\bar{b}$  resonance using either a neural network or boosted decision tree discriminant. The dominant backgrounds result from the associated production of a  $Z$  boson with jets, among which the non-resonant  $Zb\bar{b}$  production is an irreducible background. The other main backgrounds are  $t\bar{t}$ ,  $WZ$ ,  $ZZ$ , and multijet production. In order to isolate these background sources, an efficient  $b$ -tagging algorithm and a good dijet mass resolution are essential.

## II. DATA SAMPLE AND EVENT SELECTION

The DØ detector has a central-tracking system, consisting of a silicon microstrip tracker (SMT) and a central fiber tracker (CFT), both located within a 2 T superconducting solenoidal magnet [3], with tracking and vertexing at pseudorapidities  $|\eta| < 3$  and  $|\eta| < 2.5$ , respectively. A liquid-argon and uranium calorimeter has a central section (CC) covering  $|\eta|$  up to  $\approx 1.1$ , and two end calorimeters (EC) that extend coverage to  $|\eta| \approx 4.2$  [4]. An outer muon system, at  $|\eta| < 2$ , consists of a layer of tracking detectors and scintillation trigger counters in front of 1.8 T toroids, followed by two similar layers after the toroids.

This analysis is based on data which were collected between April 2002 and July 2007. The efficiency for either of the charged leptons from the  $Z$  decay to satisfy the trigger requirements is close to 100%. The integrated luminosity is found to be  $2.3 \text{ fb}^{-1}$ , after the requirement of good data quality. This conference note focuses on the the newer Run IIb data collected from June 2006 to July 2007 corresponding to an integrated luminosity of  $1.2 \text{ fb}^{-1}$ . The results of this search are then combined with the results from the Run IIa data sample [2] which uses a similar analysis methodology.

In the subsections below, we describe the event selection. A jet is reconstructed using the Run II cone algorithm with  $\Delta R = 0.5$  [5]. The jet must have  $p_T > 15 \text{ GeV}$  and a pseudorapidity of  $|\eta_{detector}| < 2.5$ . In the simulation, jets energies are smeared to reproduce the jet energy resolution observed in data. Energy scale corrections to the jets and leptons are propagated in the computation of the missing transverse energy  $\cancel{E}_T$ .

### A. Dielectron Selection

Events are required to have at least two electron candidates, with  $p_T > 15 \text{ GeV}$ ,  $|\eta_{detector}| < 1.1$  or  $1.5 < |\eta_{detector}| < 2.5$ , and that satisfy electron shower shape criteria and match to a central track. In the simulation, the electron identification efficiency is corrected as a function of  $\eta_{detector}$  and  $\phi$  for each electron to match the efficiency measured in data control samples.

A  $Z$  candidate is required, reconstructed from two electrons. The invariant mass of the electrons,  $M_{ee}$ , must be between 70 and 110 GeV. At least two jets are required in each event with each jet being isolated from both electrons by  $\Delta R > 0.5$ .

### B. Dimuon Selection

Events are required to have at least two muon candidates with  $p_T > 10 \text{ GeV}$  and  $|\eta_{detector}| < 2.0$ . The muon  $p_T$  in data is corrected using the beam spot position for muon tracks without SMT hits. In the simulation, the muon identification efficiency is corrected as a function of  $\eta_{detector}$  and  $\phi$  for each muon to match the efficiency measured in data control samples.

A  $Z$  candidate is required, reconstructed from two muons. The invariant mass of the muons,  $M_{\mu\mu}$ , must be between 70 and 130 GeV and the muons for the candidate must pass a combined isolation cut. The combined isolation is the product of the isolation variables for each of the two muons from the  $Z$  decay. The isolation for each muon is defined as:  $iso = (p_T^{track} + E_T^{calorimeter})/p_T^{muon}$ . The  $p_T^{track}$  is the sum of all tracks in a cone of  $R < 0.5$  around the muon track excluding the muon track. The  $E_T^{calorimeter}$  is the sum of all calorimeter energy in a hollow cone around the

muon from  $0.1 < R < 0.4$ . The combined isolation requirement is  $< 0.1$ . At least two jets are required in each event with no requirement on the opening angle between muons and jets.

### C. $b$ -jet Tagging

Two mutually exclusive samples are selected from data based on the number of  $b$ -tagged jets. The single-tag sample (1VT) is selected requiring that one jet passes a very tight  $b$ -tag requirement and that the second jet does not pass a loose  $b$ -tag requirement. The double-tag sample (2L) is selected requiring two jets that both pass a loose  $b$ -tag requirement. In simulation, the tag-rate-function (TRF) for data is used to predict the probability that a jet of a given flavor would be tagged. The  $b$ -tagging requirements are optimized to maximize the  $b$ -tagging efficiency while keeping the light-jet fake rate low. The resulting  $b$ -tagging efficiency for a loose tag is 72% in the central region ( $|\eta| < 0.8$ ), for  $p_T > 30$  GeV and the corresponding fake rate 4%. For a very tight tag the efficiency is 50% with a fake rate of 0.5%.

### D. Multijet Background

The background contribution from multijet processes is estimated from data. For the dielectron sample, we select a sample of events from data requiring that there be two electrons with the same sign in the event and that both fail the shower shape requirements for a good electron. We determine the normalization of the multijet background by comparing the  $e^+e^-$  invariant mass distributions of data and the sum of the multijet and the rest of the background. In the dimuon sample, the shape of the multijet background is taken from events where the combined isolation requirement is reversed ( $> 0.1$ ). This non-isolated sample is then normalized in the low dimuon mass region ( $40 < M_{\mu\mu} < 70$ ) by comparing data with the sum of all other backgrounds.

### E. Simulated Event Samples

Using the CTEQ6L1 [6] leading-order parton distribution function, the following physics processes are simulated to estimate the signal acceptance and the number of background events:  $Z(\rightarrow \ell^+\ell^-)H(\rightarrow b\bar{b})$  by PYTHIA,  $Z(\rightarrow \ell^+\ell^-)jj$  including  $Z(\rightarrow \ell^+\ell^-)c\bar{c}$  and  $Z(\rightarrow \ell^+\ell^-)b\bar{b}$  by ALPGEN,  $t\bar{t} \rightarrow e^+\nu b e^-\bar{\nu}b$  and  $t\bar{t} \rightarrow bbjje\nu$  by PYTHIA, and inclusive  $ZZ$  and  $WZ$  by PYTHIA where  $j$  stands for any light quark ( $uds$ ). The samples generated by ALPGEN [7] are interfaced with PYTHIA [8] for parton showering and hadronization. All the samples are processed using a detector simulation program based on GEANT [9], and the same reconstruction program as data.

The signal cross sections, as well as those for  $t\bar{t}$ ,  $WZ$ , and  $ZZ$  are taken from MCFM [10], which includes NLO corrections. For the ALPGEN samples, a matching procedure (MLM) is used to avoid double counting the partons produced by ALPGEN and subsequently added by PYTHIA. In addition, NLO k-factors are applied to the  $Z + nj$ ,  $Z + b\bar{b}$  and  $Z + c\bar{c}$  samples, respectively, to account for the NLO cross sections of these processes (as calculated with MCFM) as compared to the LO cross sections from ALPGEN. We assign a 30% uncertainty to the k-factors for  $Z + b\bar{b}/c\bar{c}$ . Since the  $Z p_T$  distribution is poorly modeled in  $Z + \text{jet}$  simulation, the simulated  $Z + \text{jet}$  samples are reweighted according to the measured  $Z p_T$  spectrum before  $b$ -tagging. The dielectron and dimuon invariant mass distributions for data and background after all reweighting are shown in Fig. 1. Additionally, the jet kinematic distributions for the leading and second-leading jet  $\eta$  and  $\Delta\phi(j, j)$  are poorly modeled by the ALPGEN simulation sample and so are reweighted to match the data. This reweighting procedure is similar to what has been done in other analyses using ALPGEN to describe the  $W + 2j$  background [14]. The luminosity profile of the simulated events is reweighted to match the luminosity profile of the dielectron and dimuon data sample.

## III. ANALYSIS

After requiring two electrons and two jets in the events, and  $M_{ee}$  between 70 GeV and 110 GeV but no  $b$ -tagging requirements, 3715 events are observed in data, while 3811 events are expected from the multijet plus simulated background. After requiring two muons and two jets in the events, and  $M_{\mu\mu}$  between 70 GeV and 130 GeV but no  $b$ -tagging requirements, 6250 events are observed in data, while 6256 events are expected from the multijet plus simulated background. Table I and II show the observed data and background expectations before and after  $b$ -tagging requirements.

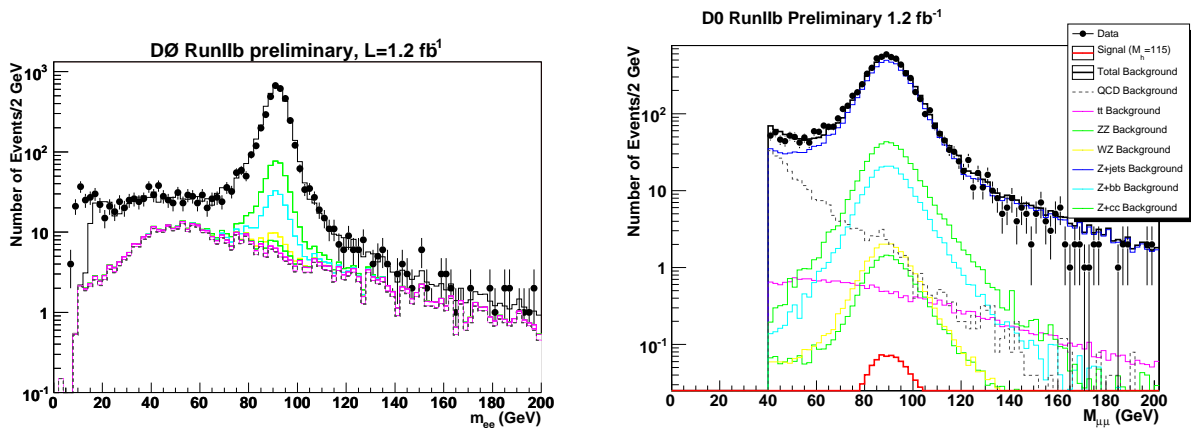


FIG. 1: The dielectron (left) and dimuon (right) invariant mass distributions. For the dielectron plot, the solid circles represent data and the red, blue, green and orange lines represent  $Z$ ,  $Z + c\bar{c}$ ,  $Z + b\bar{b}$  and multijet background, respectively. For the dimuon plots, the legend lists the sample curves.

TABLE I: The numbers of events in the dielectron sample after each requirement for data, various background processes and ZH signal, where the mass of the Higgs boson is  $m_H = 115$  GeV. The first and second errors are the statistical and systematic errors, respectively.

	pre-selection	$70 < M_{ee} < 110$ GeV	1 tight b-tag	2 loose b-tags
QCD	$481 \pm 12.6 \pm 196$	$122 \pm 3.2 \pm 49$	$3.06 \pm 0.08 \pm 1.22$	$0.84 \pm 0.02 \pm 0.33$
Z+jets	$3258 \pm 13 \pm 725$	$3167 \pm 12 \pm 705$	$9.7 \pm 0.04 \pm 2.54$	$4.1 \pm 0.02 \pm 1.10$
Z+2b	$167.0 \pm 1.1 \pm 58.4$	$162.8 \pm 1.1 \pm 56.9$	$39.8 \pm 0.3 \pm 14.0$	$17.5 \pm 0.1 \pm 6.2$
Z+2c	$335.9 \pm 2.7 \pm 119.0$	$327.1 \pm 2.6 \pm 115.9$	$18.8 \pm 0.2 \pm 6.7$	$7.19 \pm 0.06 \pm 2.60$
$t\bar{t}$	$36.5 \pm 0.5 \pm 4.6$	$11.1 \pm 0.2 \pm 1.4$	$3.1 \pm 0.04 \pm 0.40$	$3.74 \pm 0.05 \pm 0.58$
WZ	$13.4 \pm 0.1 \pm 3.5$	$12.8 \pm 0.1 \pm 3.3$	$0.43 \pm 0.004 \pm 0.09$	$0.11 \pm 0.001 \pm 0.03$
ZZ	$10.0 \pm 0.1 \pm 2.5$	$9.0 \pm 0.1 \pm 2.2$	$0.71 \pm 0.01 \pm 0.15$	$0.63 \pm 0.01 \pm 0.15$
Tot Bkg	$4301 \pm 18 \pm 762$	$3811 \pm 13 \pm 718$	$75.6 \pm 0.3 \pm 15.8$	$34.1 \pm 0.1 \pm 6.9$
ZH	$0.77 \pm 0.01 \pm 0.10$	$0.74 \pm 0.01 \pm 0.09$	$0.21 \pm 0.002 \pm 0.03$	$0.24 \pm 0.003 \pm 0.04$
Data	4512	3715	80	40

### A. Multivariate Discriminant Analysis

In order to take full advantage of the kinematic information in the data, we use a multivariate discriminant analysis to search for the Higgs boson. In the electron channel, we train a neural network (NN) using the following 10 variables: the invariant mass of two jets (the two  $b$ -tagged jets in 2L4 sample, or the tight  $b$ -tagged jet and the leading  $p_T$  non  $b$ -tagged jet in the 1VT sample),  $p_T$  of the leading jet,  $p_T$  of the second leading jet,  $\Delta R$  between the two electrons,  $\Delta\eta$  between the two jets,  $\Delta\phi$  between the two jets,  $\Delta R$  between the leading jet and the  $Z$ ,  $\eta$  of the  $Z$ , the missing transverse energy of the event, and the total scalar energy in the event. Some of the input distributions for the NN discriminant are shown in Figs. 2 – 3. We train the NN for each Higgs boson mass point, and for the single-tag and the double-tag samples separately. The NN output distributions are shown in Fig. 4.

In the muon channel, we train a boosted decision tree (BDT) using the same variables used for the NN and the following additional set of variables:  $p_T$  and  $\eta$  of the leading and second leading muons,  $p_T$  and invariant mass of the  $Z$ ,  $\Delta\eta$  and  $\Delta\phi$  between the  $Z$  and the leading jet,  $\eta$  of the leading and second leading jet, acoplanarity and collinearity of the  $Z$  muons, and the number of jets in the event. The input distributions of several of the most significant variables for the BDT discriminant are shown in Figs. 5 – 6. We train the BDT for each Higgs boson mass point, and for the single-tag and the double-tag samples separately. The BDT output distributions are shown in Fig. 7.

### B. Systematic Uncertainties

The systematic uncertainties due to data/MC differences in the distributions of the dijet invariant mass, and of the missing  $E_T$  are taken into account in the limit calculation program, considering also the effects on the shape of the

TABLE II: The numbers of events in the dielectron sample after each requirement for data, various background processes and ZH signal, where the mass of the Higgs boson is  $m_H = 115$  GeV. The first and second errors are the statistical and systematic errors, respectively.

	pre-selection	$70 < M_{\mu\mu} < 110$ GeV	1 tight b-tag	2 loose b-tags
Multijet	$261 \pm 10 \pm 125$	$48.9 \pm 3.2 \pm 24.4$	$4.80 \pm 0.07 \pm 2.40$	$3.61 \pm 0.01 \pm 1.8$
Z+jets	$6215 \pm 22 \pm 740$	$5441 \pm 20 \pm 630$	$23.7 \pm 0.12 \pm 4.5$	$17.7 \pm 0.08 \pm 3.1$
Z+2b	$247 \pm 1.5 \pm 74$	$235 \pm 1.8 \pm 63$	$55.4 \pm 0.4 \pm 21.1$	$28.3 \pm 0.2 \pm 10.7$
Z+2c	$504 \pm 3.6 \pm 155$	$479 \pm 3.5 \pm 145$	$27.3 \pm 0.2 \pm 6.0$	$13.3 \pm 0.11 \pm 5.4$
$t\bar{t}$	$28.5 \pm 0.3 \pm 4.0$	$12.9 \pm 0.2 \pm 1.7$	$3.4 \pm 0.04 \pm 0.40$	$4.6 \pm 0.04 \pm 0.63$
WZ	$25.0 \pm 0.1 \pm 2.6$	$23.2 \pm 0.1 \pm 2.5$	$0.76 \pm 0.01 \pm 0.09$	$0.30 \pm 0.01 \pm 0.05$
ZZ	$18.3 \pm 0.15 \pm 1.9$	$16.6 \pm 0.14 \pm 1.9$	$1.25 \pm 0.01 \pm 0.15$	$1.24 \pm 0.01 \pm 0.15$
Tot Bkg	$7297 \pm 24 \pm 850$	$6256 \pm 23 \pm 823$	$116.6 \pm 0.5 \pm 24.0$	$69.0 \pm 0.3 \pm 18.2$
ZH	$0.95 \pm 0.01 \pm 0.10$	$0.87 \pm 0.01 \pm 0.09$	$0.23 \pm 0.002 \pm 0.025$	$0.29 \pm 0.002 \pm 0.03$
Data	7262	6250	117	67

multivariate output. Similarly the uncertainties due to the jet energy scale, b-tagging probabilities, Z  $p_T$  reweighting, jet  $\eta$  reweighting, and  $\Delta\phi(j, j)$  reweighting are considered by generating the multivariate output for MC samples corresponding to  $\pm 1\sigma$  variations of the reference parametrizations of these effects.

Other systematic uncertainties included in the calculation are the uncertainties for the luminosity measurement, the electron identification, the muon identification, the theoretical cross sections for the background processes and the estimate for the multijet background. These uncertainties affect only the overall normalization of each background sample. We use 6.1% for the uncertainty of the luminosity measurement [11]. Based on the uncertainties for the correction factors for the electron preselection and for the electron selection per electron, we assign a 4% systematic error. The uncertainty on the corrections to the muon selection efficiency is 2% systematic error. The uncertainty for the multijet background is taken from the error on the multijet scale factor and is estimated to be 41% for the dielectron sample and 50% for the dimuon sample. Uncertainties of 10% are assigned to the theoretical cross sections, except for the  $Z+b\bar{b}/c\bar{c}$  processes, for which we use uncertainties of 30%.

### C. Results

We set limits on the  $ZH$  cross section using the modified frequentist (CLs) method using a log-likelihood test statistic [12, 13]. The histograms of the multivariate analysis output for the single-tag and the double-tag samples are the input for the limit setting program. The histograms for the systematic uncertainties mentioned above are used in the program, along with the constant systematic uncertainties. The effect of the systematics is minimised using the profile likelihood technique [13]. The expected and observed cross section limits in the dielectron sample are listed in Table III and plotted in Fig. 8 along with the log-likelihood ratio from the CLs method. The expected and observed cross section limits in the dimuon sample are listed in Table IV and plotted in Fig. 9 along with the log-likelihood ratio (LLR) from the CLs method. The limits on the cross section for Higgs boson of mass 115 GeV are about 25-30 times the standard model cross section. Combining the electron and muon channels in the Run IIb data, the observed cross section limit for a Higgs mass of 115 GeV is 20 times the standard model prediction. A combination of these results with the Run IIa produces a cross section limit of 11 times the standard model cross section prediction.

TABLE III: The limits on the cross section based on the multivariate discriminant and the CLs method for the Run IIb sample.

$m_H$ (GeV)	Dielectron				Dimuon			
	Exp(pb)	(Exp/SM)	Obs(pb)	(Obs/SM)	Exp(pb)	(Exp/SM)	Obs(pb)	(Obs/SM)
100	4.14	(30.5)	3.35	(19.9)	4.09	(24.3)	3.89	(23.1)
105	5.33	(36.9)	3.82	(26.4)	3.25	(22.5)	3.56	(24.6)
110	4.51	(36.2)	3.39	(27.2)	3.69	(28.5)	3.95	(30.5)
115	4.76	(44.2)	3.47	(32.2)	3.34	(31.0)	3.60	(33.4)
120	4.53	(48.4)	3.19	(34.1)	3.16	(33.8)	3.83	(40.9)
125	4.48	(55.0)	2.60	(32.0)	3.11	(38.2)	3.94	(48.4)
130	5.05	(71.1)	4.19	(58.3)	3.35	(47.1)	4.41	(62.0)
135	5.98	(96.1)	4.50	(72.3)	3.53	(56.8)	4.31	(69.3)
140	7.43	(135.8)	4.92	(89.9)	4.49	(82.1)	6.62	(121)

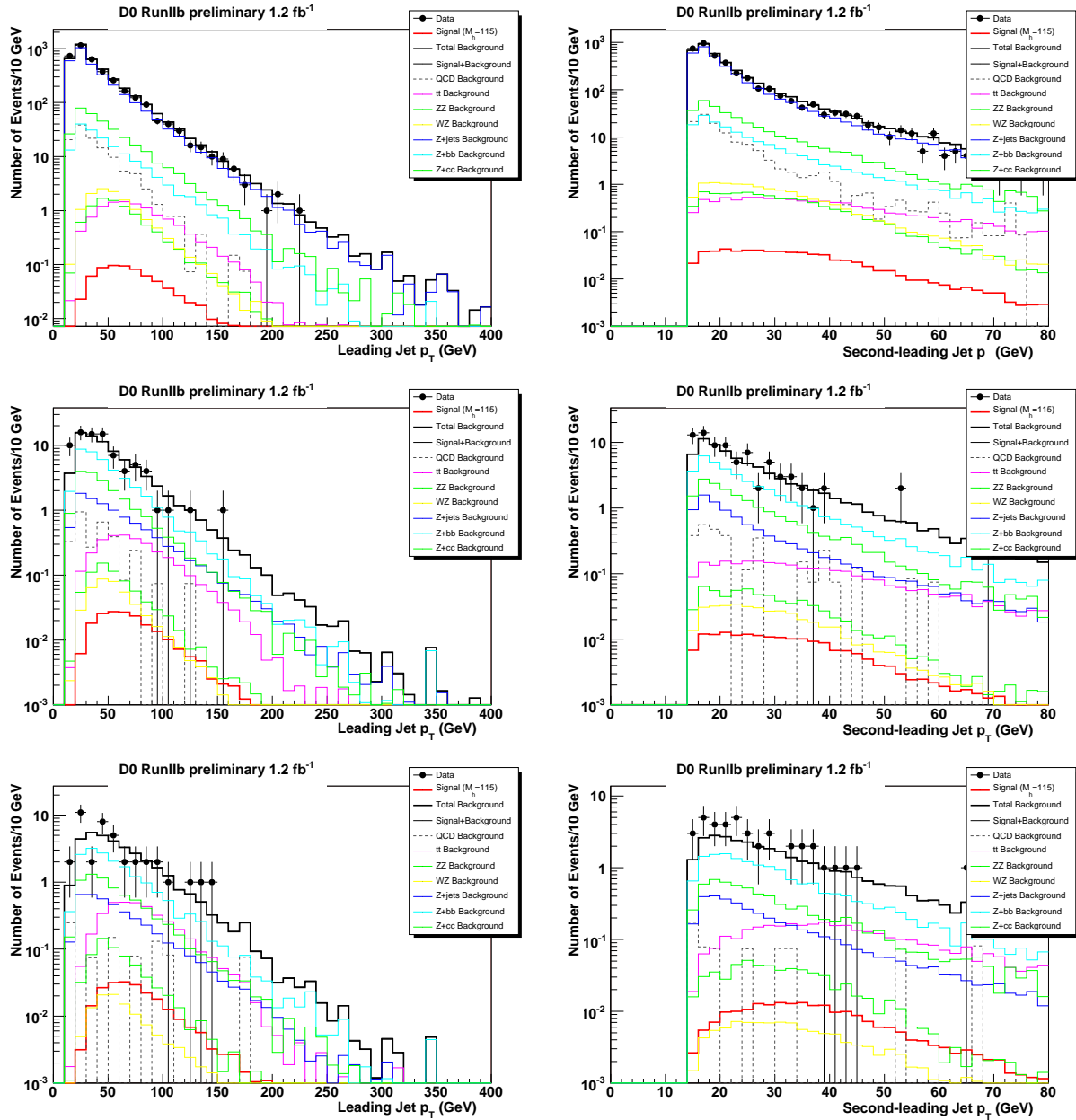


FIG. 2: The leading jet  $p_T$  (left column) and the second-leading jet  $p_T$  (right column) distributions in the dielectron sample. The top row shows the plots for the pre-tag sample. The middle and bottom rows show single- and double- tag sample, respectively.

#### IV. SUMMARY

A search for a Higgs boson produced in association with a  $Z$  boson in  $p\bar{p}$  collisions at  $\sqrt{s} = 1.96$  TeV at the Fermilab Tevatron collider is performed, using  $1.2 \text{ fb}^{-1}$  of data. Events with a  $Z \rightarrow \ell^+\ell^-$  and two jets where at least one jet is  $b$ -tagged are selected. The observed data are consistent with the expected background. Upper limits on the  $ZH$  production cross section are set for Higgs masses between 100 and 140 GeV. The limits on the cross section for a Higgs boson of mass of 115 GeV are about 25-30 times the standard model prediction for both dielectron and dimuon Run IIb analyses. The combined limit on the cross section in the Run IIb sample is 20, and when combined with the Run IIa data, the limit for the full Run II dataset is about 11 times the standard model prediction for a  $m_H = 115$  GeV.

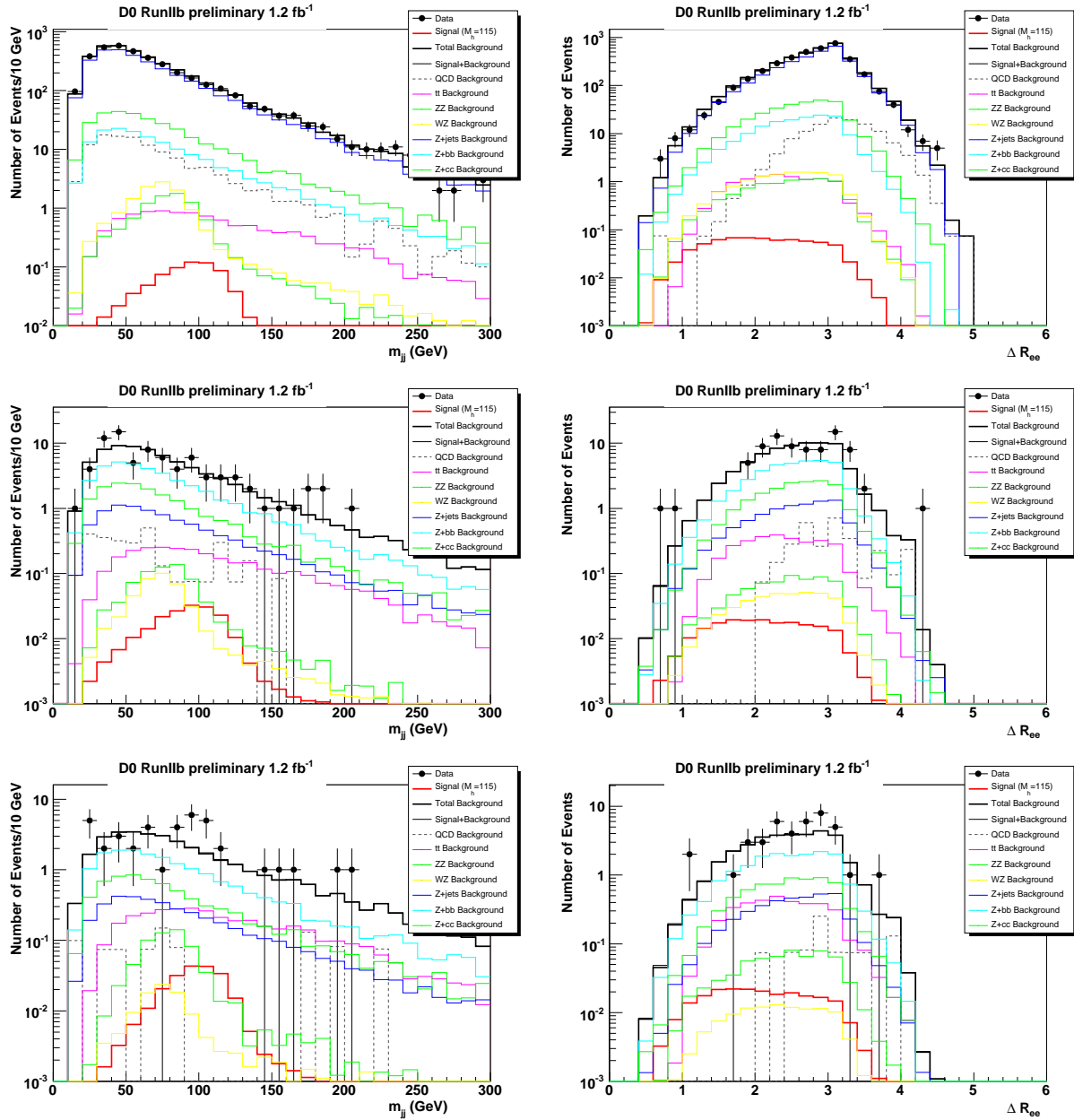


FIG. 3: The dijet invariant mass (left column) and the  $\Delta R(e, e)$  (right column) distributions in the dielectron sample. The top row shows the plots for the pre-tag sample. The middle and bottom rows show single- and double- tag sample, respectively.

### Acknowledgments

We thank the staffs at Fermilab and collaborating institutions, and acknowledge support from the DOE and NSF (USA); CEA and CNRS/IN2P3 (France); FASI, Rosatom and RFBR (Russia); CAPES, CNPq, FAPERJ, FAPESP and FUNDUNESP (Brazil); DAE and DST (India); Colciencias (Colombia); CONACyT (Mexico); KRF and KOSEF (Korea); CONICET and UBACyT (Argentina); FOM (The Netherlands); STFC (United Kingdom); MSMT and GACR (Czech Republic); CRC Program, CFI, NSERC and WestGrid Project (Canada); BMBF and DFG (Germany); SFI (Ireland); The Swedish Research Council (Sweden); CAS and CNSF (China); and the Alexander von Humboldt

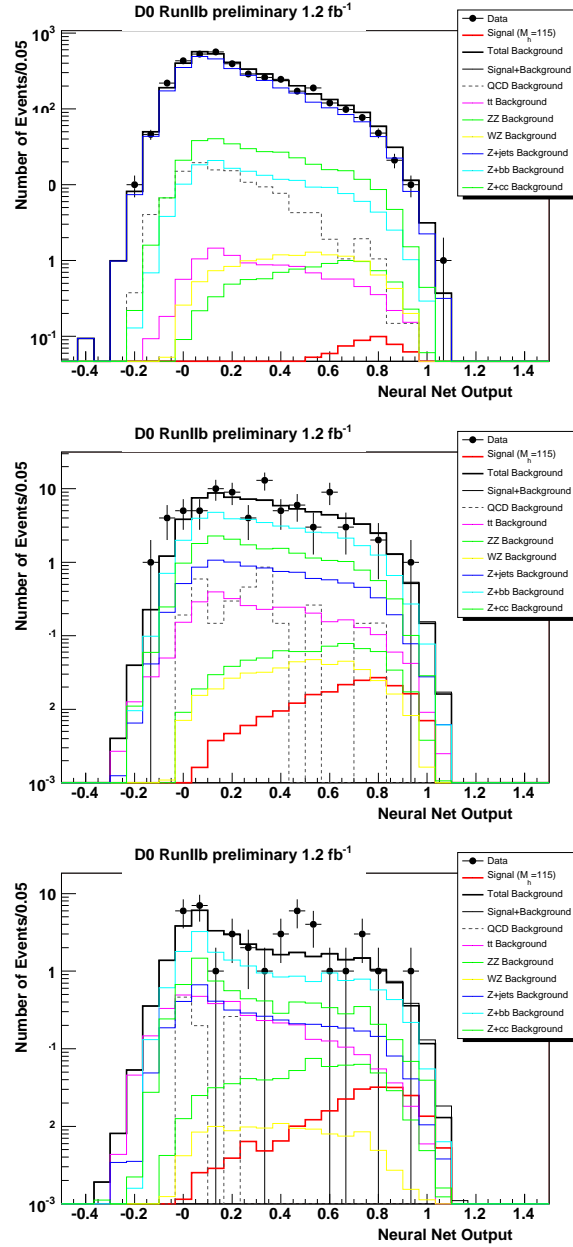


FIG. 4: The multivariate discriminant output distributions for the dielectron sample. The multivariate discriminant is trained for the Higgs mass of 115 GeV. The top plot shows the distribution for the pre-tag sample, and the middle and the bottom are for the single- and double- tag sample, respectively.

Foundation.

- 
- [1] T. Han and S. Willenbrock, Phys. Lett. B273 (1991) 167. A.Djouadi, J.Kalinowski and M.Spira, Comp. Phys. Commun. 108 C (1998) 56, hep-ph/9704448.
  - [2] DØ Collaboration, "Search for  $ZH \rightarrow \ell\ell b\bar{b}$  in  $p\bar{p}$  collisions at  $\sqrt{s} = 1960$  GeV", <http://www-d0.fnal.gov/Run2Physics/WWW/results/prelim/HIGGS/H39/H39.pdf>
  - [3] DØ Collaboration, V. Abazov *et al.*, "The Upgraded DØ Detector," Nucl. Instrum. Methods Phys. Res. A **565**, 463 (2006).
  - [4] S. Abachi, *et al.*, Nucl. Instrum. Methods Phys. Res. A **338**, 185 (1994).
  - [5] G. C. Blazey *et al.*, in *Proceedings of the Workshop: "QCD and Weak Boson Physics in Run II,"* edited by U. Baur,

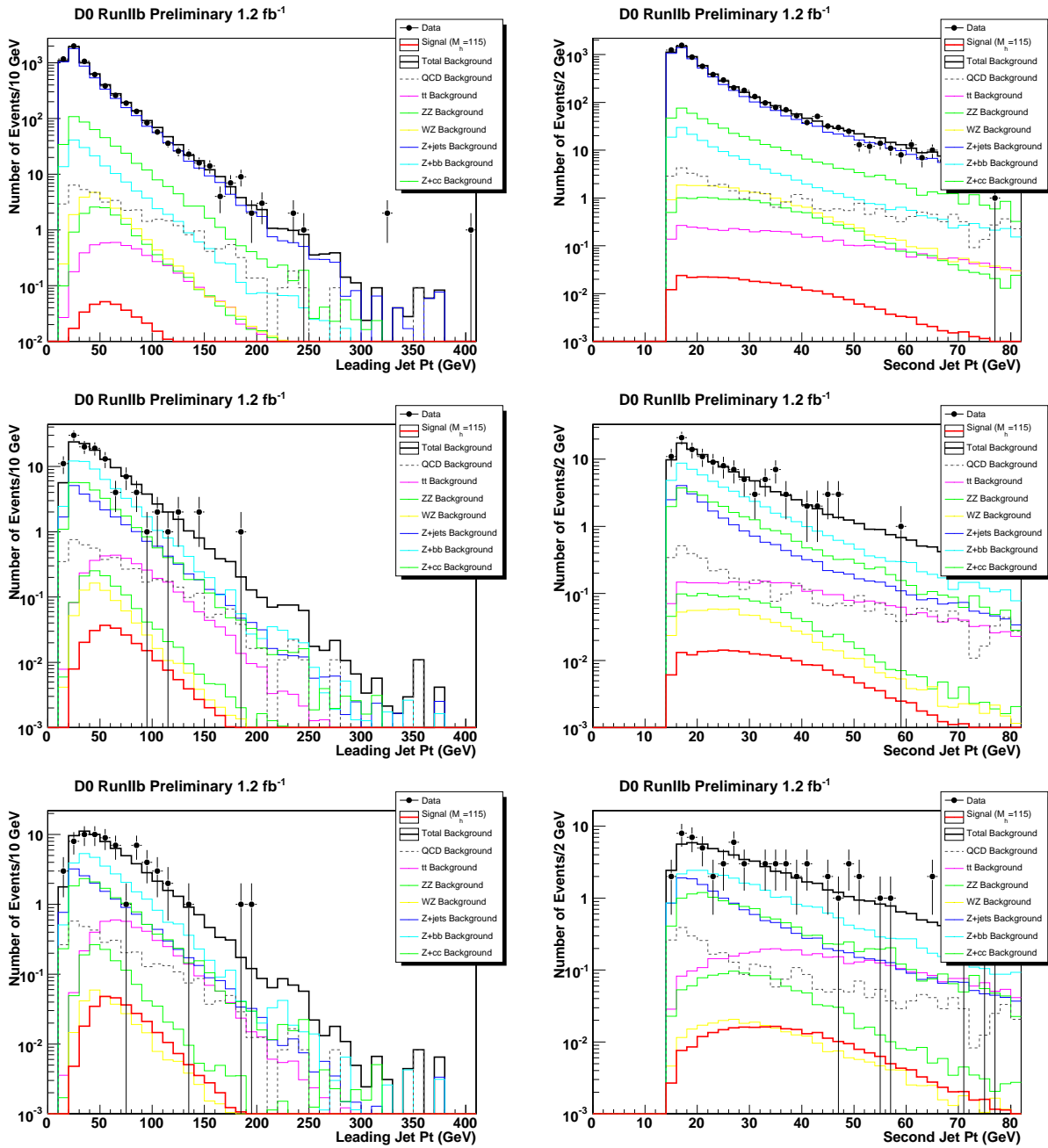


FIG. 5: The leading jet  $p_T$  (left column) and the second-leading jet  $p_T$  (right column) distributions in the dimuon sample. The top row shows the plots for the pre-tag sample. The middle and bottom rows show single- and double- tag sample, respectively.

R. K. Ellis, and D. Zeppenfeld, (Fermilab, Batavia, IL, 2000) p. 47; see Sec. 3.5 for details.

- [6] J. Pumplin et al., J. High Energy Phys. 07 (2002) 012.
- [7] M. L. Mangano et al., JHEP 0307, 001 (2003).
- [8] T. Sjostrand et al., Comput. Phys. Commun. 135, 238 (2001).
- [9] R. Brun, F. Carminati, CERN Program Library Long Writeup W5013 (1993).
- [10] J. Campbell and K. Ellis, MCFM, *Monte Carlo for FeMtobarn processes*, <http://mcfm.fnal.gov/>.
- [11] T. Andeen et al., FERMILAB-TM-2365 (2007).
- [12] T. Junk, Nucl. Instrum. Methods Phys. Res., Sect. A **434**, 435 (1999); A. L. Read, Workshop on Confidence Limits, CERN-OPEN-2000-205 (2000).
- [13] W. Fisher, FERMILAB-TM-2386-E (2007).

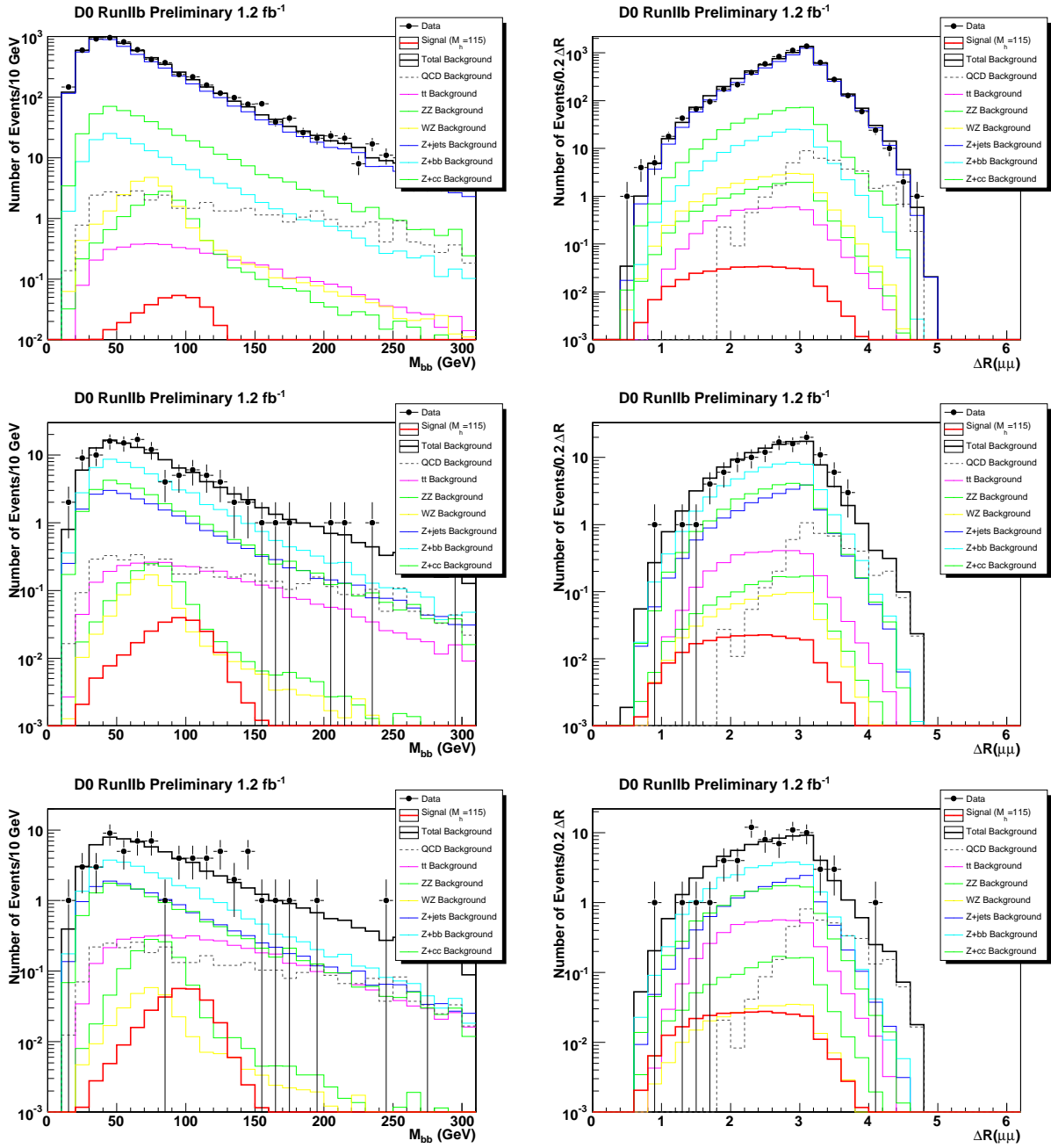


FIG. 6: The dijet invariant mass (left column) and the  $\Delta R(e, e)$  (right column) distributions in the dimuon sample. The top row shows the plots for the pre-tag sample. The middle and bottom rows show single- and double- tag sample, respectively.

[14] The DØ Collaboration, "A Search for Associated W and Higgs Production in p-anti-p Collisions at  $\sqrt{s}=1.96$  TeV", <http://www-clued0.fnal.gov/gregorio/WH-pdf/prl-p17.pdf>

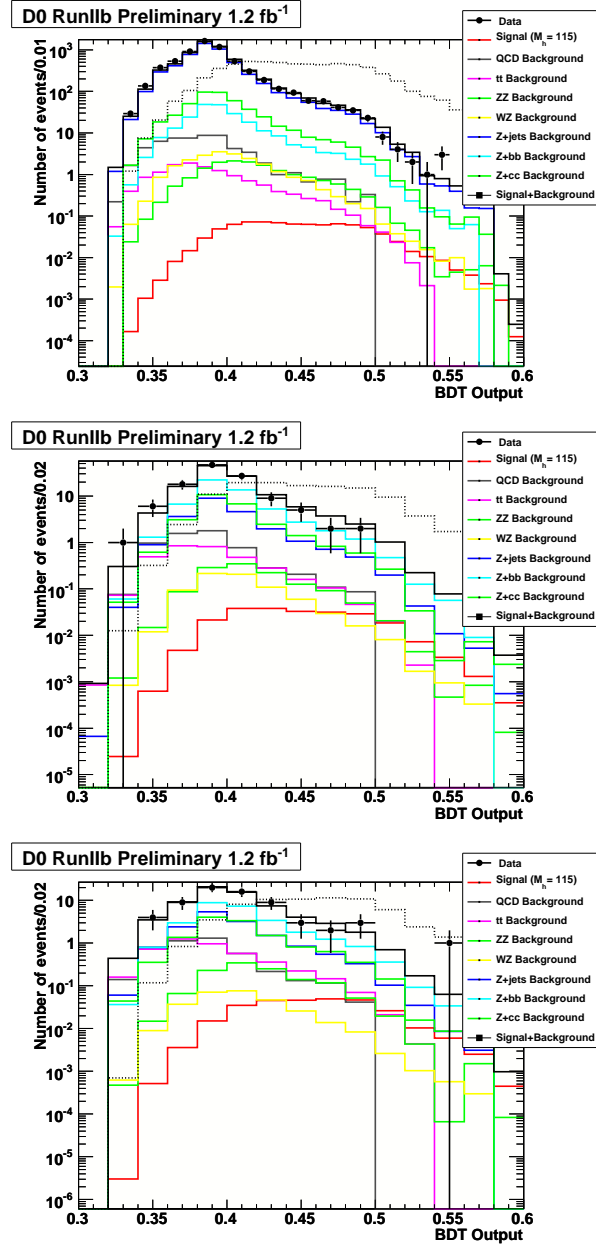


FIG. 7: The multivariate output distributions for the dimuon sample. The multivariate discriminant is trained for the Higgs mass of 115 GeV. The top plot shows the distribution for the pre-tag sample, and the middle and the bottom are for the single- and double- tag sample, respectively. To show the discriminating power of the discriminant, the dashed line shows the ZH signal response when normalized to equal area of the background.

TABLE IV: The combined limits on the  $ZH$  production cross section as a ratio to the standard model prediction based on the multivariate discriminant and the CLs method in the combined Run IIa, combined Run IIb, and the full RunII sample.

Mass	Comb Run IIa		Comb Run IIb		Comb Run II	
	Obs	Exp	Obs	Exp	Obs	Exp
100			12.5	14.3	5.94	9.05
105	11.2	14.9	16.2	15.6	6.90	9.88
110			17.1	16.9	7.79	10.9
115	17.8	20.4	20.2	19.3	11.0	12.3
120			22.9	21.4	16.5	14.0
125	30.4	27.3	21.1	24.9	16.1	16.7
130			34.5	32.1	23.3	21.0
135	51.4	42.8	42.9	40.0	32.1	26.9
140			59.9	57.5	39.5	38.0

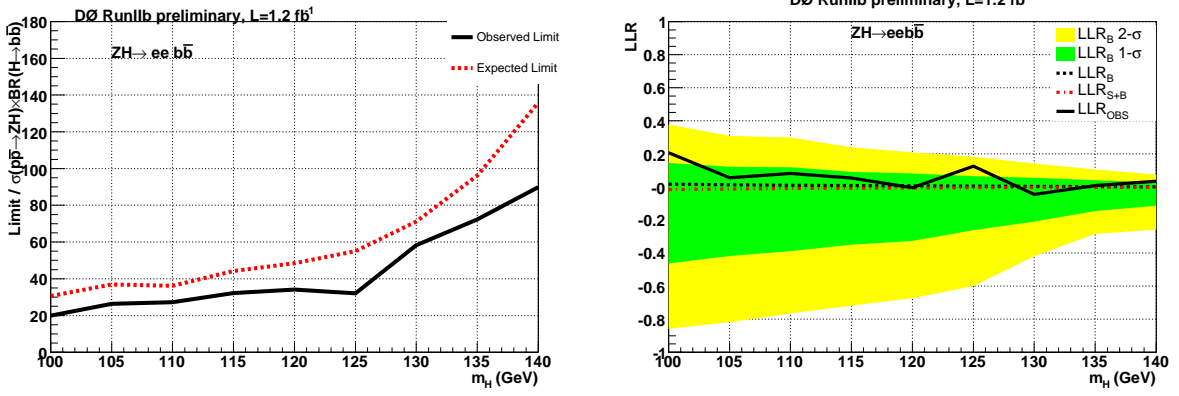


FIG. 8: The cross section limits based on the multivariate discriminant and the CLs method in the Run IIb dielectron sample. The left plot shows the expected and observed cross sections divided by the SM prediction. The right plot shows the log-likelihood ratio from the CLs method.

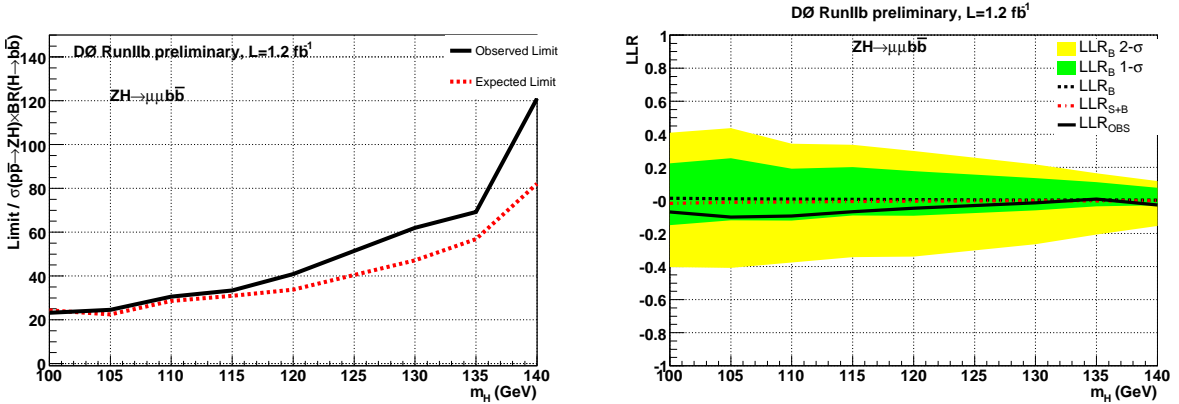


FIG. 9: The cross section limits based on the multivariate discriminant and the CLs method in the Run IIb dimuon sample. The left plot shows the expected and observed cross section limits divided by the SM prediction. The right plot shows the log-likelihood ratio from the CLs method.

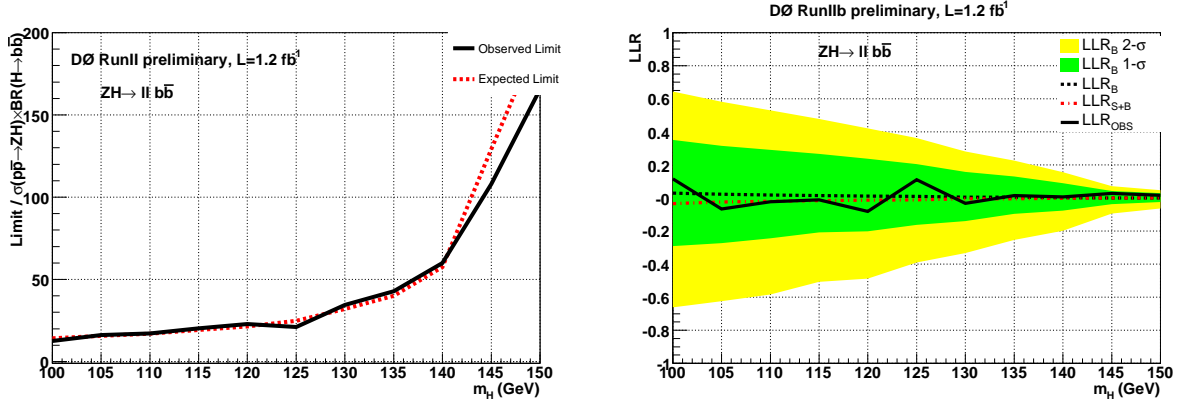


FIG. 10: The cross section limits based on the multivariate discriminant and the CLs method in the combined dielectron and dimuon Run IIb sample. The left plot shows the expected and observed cross section limits divided by the SM prediction. The right plot shows the log-likelihood ratio from the CLs method.

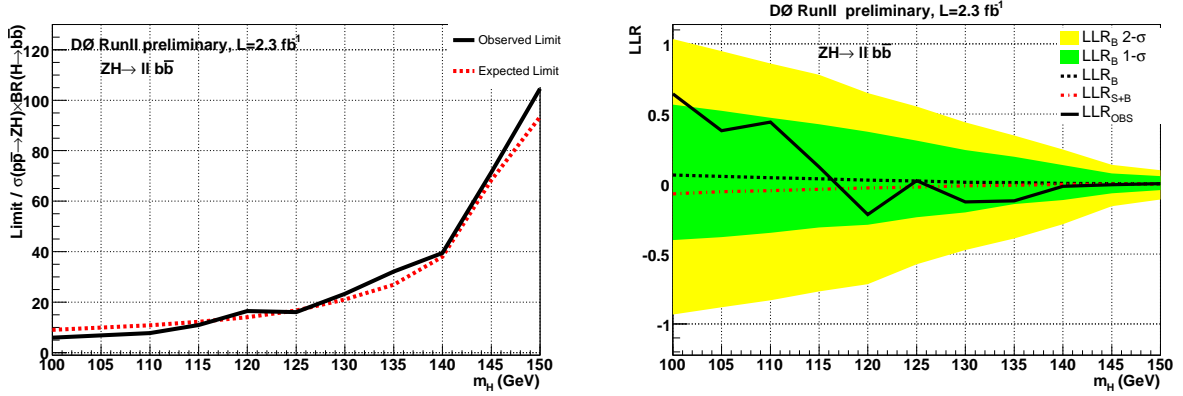


FIG. 11: The cross section limits based on the multivariate discriminant and the CLs method in the combined dielectron and dimuon full Run II sample. The left plot shows the expected and observed cross section limits divided by the SM prediction. The right plot shows the log-likelihood ratio from the CLs method.